Journal of Hazardous Materials 203–204 (2012) 308–316

Contents lists available at SciVerse ScienceDirect

Journal of Hazardous Materials

journal homepage: www.elsevier.com/locate/jhazmat

Identification and chemical characterization of particulate matter from wave soldering processes at a printed circuit board manufacturing company

Z. Szoboszlai[a,*], Zs. Kertész[a], Z. Szikszai[a], A. Angyal[a], E. Furu[a], Zs. Török[a], L. Daróczi[b], Á.Z. Kiss[a]

[a] Institute of Nuclear Research of the Hungarian Academy of Sciences (ATOMKI), H-4001 Debrecen, P.O. Box 51, Hungary
[b] Department of Solid State Physics, University of Debrecen, H-4010 Debrecen, P.O. Box 2, Hungary

ARTICLE INFO

Article history:
Received 29 August 2011
Received in revised form
25 November 2011
Accepted 10 December 2011
Available online 19 December 2011

PACS:
82.80.Ej
82.80.Yc
92.60.Sz
68.37.Yz

Keywords:
Wave soldering
Workplace aerosol
Ion beam analysis
PIXE
Single particle analysis

ABSTRACT

In this case study, the elemental composition and mass size distribution of indoor aerosol particles were determined in a working environment where soldering of printed circuit boards (PCB) took place. Single particle analysis using ion and electron microscopy was carried out to obtain more detailed and reliable data about the origin of these particles. As a result, outdoor and indoor aerosol sources such as wave soldering, fluxing processes, workers' activity, mineral dust, biomass burning, fertilizing and other anthropogenic sources could be separated. With the help of scanning electron microscopy, characteristic particle types were identified. On the basis of the mass size distribution data, a stochastic lung deposition model was used to calculate the total and regional deposition efficiencies of the different types of particles within the human respiratory system. The information presented in this study aims to give insights into the detailed characteristics and the health impact of aerosol particles in a working environment where different kinds of soldering activity take place.

1. 1.Introduction

Several studies have shown that aerosol particles have a negative impact on human health [1–3]. The risk from the inhaled particles depends on their chemical composition, their size distribution as well as their deposition in the human respiratory system. Research of particulate matter (PM) toxicity has shown that, in general, the smaller PM size fractions (<PM_{10}) have the highest toxicity through containing higher concentrations of extractable organic matter (comprising a wide spectrum of chemical substances), and possessing a relatively high radical-generating capacity [4,5]. Since smaller particles have a larger surface area, these particles can transport a greater amount of toxins into the lower respiratory tract, leading to more adverse health effects [6]. In workplaces fine and ultrafine particles are often associated with anthropogenic activities such as soldering, smelting, welding and spraying [7–10].

It is well known that the electronics products industry has exposed workers to high doses of metals [11]. Several studies have reported that the inhalation of metal dust and fumes is associated with adverse health effects such as metal fume fever and other respiratory diseases [12–14]. Quansah·and Jaakkola [13] have shown that maternal exposure to metal dust or fumes during pregnancy may reduce fetal growth. They also implied that paternal exposure to welding fumes may increase the risk of preterm delivery and small-for-gestational age. Because of these facts it is crucial to analyse PM (with metal content) in environments where people are working in a restricted space during long periods of time.

Tin is the most abundant heavy metal used in soldering processes. An adverse health effect on workers exposed to tin oxide from the smelting or production of tin has been observed in studies and it has been documented as stannosis [14]. Through the occupational contamination of clothing, tin can also appear in indoor dust at the homes of the workers [15]. Lead, one of the most toxic metals that can appear in this kind of workplace, affects the brain and the nervous, renal, reproductive and cardiovascular systems (e.g. a review by Chang, [16] and Golub [17]). Long-term exposure to

* Corresponding author at: Institute of Nuclear Research of the Hungarian Academy of Sciences (ATOMKI), H-4026 Debrecen, Bem tér 18/c, Hungary.
Tel.: +36 52 509 200; fax: +36 52 416 181.
E-mail address: szoboszlai@atomki.hu (Z. Szoboszlai).

0304-3894/$ – see front matter © 2011 Elsevier B.V. All rights reserved.
doi:10.1016/j.jhazmat.2011.12.030

lead can cause nephropathy and colic-like abdominal pains, and can result in decreased performance in certain tests that measure functions of the nervous system [18]. According to Lilis et al. [19], lead containing indoor PM induced biological effects on workers. However, most studies dealing with lead-containing PM have focused on the environmental effect of outdoor aerosols and only a few of them have dealt with indoor PM collected at workplaces.

To the best of our knowledge, there is as yet no study concerning the chemical composition and the mass size distribution of PM originating from wave soldering processes.

In this case study our aim was to determine the parameters which might help to better estimate the impact on human health in a workplace where the soldering and testing of different kinds of printed circuit boards (PCBs) and other electronic components takes place. Wave soldering is one of the main processes used for attaching metal components to the board during the manufacturing of PCBs [20]. The name is derived from the use of waves of molten solder. The constituents of the solder alloy are dependent on the type of wave solder e.g. leaded (Sn–Pb) or lead free wave solder (Sn–Ag–Cu–Sb) [21]. Since lead is one of the common solder alloys, knowledge of the workers' exposure to this element was particularly important. We utilized a stochastic lung model to calculate the total and regional deposition efficiencies of the different types of particles within the human respiratory system (in the case of different activities: sitting and manual work) [22–24].

2. Experimental

2.1. Sampling

Two 48-h long sampling campaigns were carried out. One was in October 2008 and the other was in May 2009. Aerosol samples were collected in a large working hall where approximately 100 people (male and female) worked. In this working environment the production, soldering, and testing of different kinds of PCB and other electronic components took place. Hence several supply air ventilators operated continuously during working hours, ensuring that only filtered air got into the hall. During the first sampling in 2008 the employees worked around the clock but during the second sampling campaign in 2009 there were only two shifts. From 2008 to 2009 some of the leaded wave solders were put out of operation or switched to lead-free alternatives.

Two different sampling devices were used at the above-mentioned work location. One was Nuclepore two-stage samplers. This sampling head collects the aerosol particles in two size fractions: the fine ($PM_{2.5}$= particles with aerodynamic diameter less than 2.5 μm) and coarse ($PM_{2.5-10}$= particles with aerodynamic diameter bigger than 2.5 μm). Two Nuclepore polycarbonate filters with 8 μm and 0.4 μm pore diameter are placed one behind the other in the sampling head, and the air is pumped through this system with 250–300 l/min flow rate. Coarse particles are deposited on the filter with 8 μm pore diameter, while fine particles passes through its pores, and are collected on the other filter.

In addition, a ten-stage PIXE International cascade impactor [25] was used to provide size resolved samples in the following ten fractions >16, 16–8, 8–4, 4–2, 2–1, 1–0.5, 0.5–0.25, 0.25–0.12, 0.12–0.06 and <0.06 μm aerodynamic diameter. These samples were collected on kapton foils. In the first campaign the sampling was done next to a lead-free wave solder equipment (the main constituent of the melt were Sn, Ag and Cu), at a height of 1.5 m above ground. During the second sampling campaign, in addition to the previous spot, samples were collected at 3 other sites in order to obtain information about the distribution of the aerosols in the hall. Aerosol samples were collected in the following sites: next to 2 wave solders (in one of them unleaded and in the other leaded melt was used), below a supply air ventilator and close to a location named "store of hazardous materials". The two wave solders (leaded and unleaded) were approximately 10 m apart from each other. The ten-stage PIXE International cascade impactor was only used at the ULWS in both campaigns. Outdoor aerosol samples were also collected parallel to the campaigns in an urban background site, the garden of ATOMKI, approximately 4 km away from the workplace. This sampling was carried out with a two stage Gent stacked [26] filter unit equipped with Nuclepore polycarbonate filters of 8 μm diameter and 0.4 μm pore size.

2.2. Analysis

The total mass concentration was determined by gravimetry. The aerosol filters were conditioned at least 24 h before weighing in the weighing room at 24 °C temperature and 56% relative humidity.

The analytical quantification of aerosols was done by the particle-induced X-ray emission (PIXE) method. PIXE is based on the detection of characteristic X-rays induced by a 2–3 MeV energy proton beam. PIXE is a widely applied multielemental analytical technique in atmospheric aerosol research [27].

The elemental compositions (for $Z \geq 13$) of the bulk samples were measured in the PIXE chamber installed on the left 45° beamline of the 5 MV Van de Graaff accelerator in the IBA Laboratory of ATOMKI. The details of the setup are reported here [28]. The samples were irradiated with a proton beam of 2 MeV energy. The beam spot had a diameter of 5 mm. The beam intensity was typically 40 nA, and the accumulated charge on each sample was 40 μC.

Samples collected with the impactor were further analysed by ion microscopy at the Debrecen scanning ion microprobe facility [29,30]. In this case, the samples were irradiated and scanned by a focused (1.5 μm × 1.5 μm) proton beam. The proton energy was 2 MeV. The concentration and distribution of the elements were determined by light element PIXE and PIXE techniques [31,32].

Additional elemental and morphological analysis was performed using a HITACHI S-4300 CFE scanning electron microscope at the Department of Solid State Physics, University of Debrecen. The SEM analysis was carried out on selected samples where the concentration of Sn or Pb was high. Since the applied nuclear analytical techniques are non-destructive, the same samples were used for the SEM analysis. These were the kapton foil of 0.5–1.0 μm size fraction in the impactor and the coarse fraction ($PM_{2.5-10}$) filters.

2.3. Data evaluation

In the case of bulk PIXE measurements, the evaluation of the X-ray spectra was done with the PIXECOM program package [33]. In the case of the ion microprobe measurements, signals from all detectors were recorded in list mode files by the Oxford type data acquisition system (OMDAQ) [34]. The spectra were evaluated with the PIXEKLM-TPI computer code reckoning with the thickness (size) of the particles [35].

On the basis of the obtained data, the total and regional deposition efficiencies of the different types of particles within the human respiratory system were calculated by using the newest version of the IDEAL stochastic lung deposition model [36,37]. This model is under continuous development and it was originally developed by Koblinger and Hofmann [22–24]. The ratio of deposited particles in the extrathoracic, tracheobronchial and the acinar regions was calculated for an adult male and female under sitting and light exercise breathing conditions. The stochastic term means that this model use Monte Carlo simulations to generate several geometric parameters: generation number, diameter of airways, length of airways, diameter of daughter branches, length of daughter branches, branching angles. To calculate particle trajectories, the model takes into consideration the main deposition mechanisms, that is inertial

impaction, gravitational settling and Brownian motion. Deposition of particles is computed by analytical equations (detailed descriptions are in [22]). To evaluate the regional depositions the required lung parameters (for example tidal volume, functional residual capacity, etc.) were adopted from (ICRP, 1994) [38]. The necessary element frequency in a given aerosol size range were adopted from the mass size distributions data (determined with the cascade impactor).

3. Results and discussion

3.1. Elemental concentrations

Coarse and fine PM and elemental concentration data are given in Table 1 and Table 2 respectively. In the following, the leaded wave solder will be referred to as LWS, the unleaded wave solder as ULWS, the supply air ventilator as SAV and the "store of hazardous materials" as SHM. Since it was not possible to collect outdoor samples at the company, samples collected in the garden of ATOMKI, which is a similar urban background site, were used for comparison. The PM_{10} concentration values measured by us (in the ATOMKI) were similar to the values observed at two other urban background sites in Debrecen (measured by the Hungarian air quality monitoring system [39]) in both campaigns. In October 2008: the total mass concentrations were 25.1 $\mu g/m^3$ at ATOMKI and 27.6 $\mu g/m^3$ and 28 $\mu g/m^3$ at the official stations. In May 2009: 16.8 $\mu g/m^3$ was measured at ATOMKI and 16.0 g/m^3 and 16.6 $\mu g/m^3$ at the official stations. The differences between the concentration values measured in 2008 and 2009 can be explained by the different meteorological conditions (in May 2009 it was rainy) and by human activity (e.g. domestic heating in October 2008).

The concentrations measured indoors were higher in 2008 than in 2009. This is in relation with the working conditions. The employees worked around the clock in 2008 while during the second sampling campaign there were only two shifts so the dust had time to settle down.

The presence of soil-derived elements (like Si, Al, Ca and Ti) in the working hall indicated that in spite of the filtering equipment outdoor pollution could reach the hall through the supply air ventilators. The similar indoor/outdoor ratios of these elements in both size fractions below the SAV (e.g. this ratio is 0.12 either for fine and coarse fraction Si or Ca) implies that the supply air ventilator filters the fine and coarse fraction with similar efficiency. On the other hand, the indoor/outdoor ratios for P, S, Cl K, Mn, Fe, Cu, Zn, and Pb elements were higher than the crust-related elements. This suggests that there were also sources of these elements inside the workplace.

Among the measured elements Sn, Ag, Br and Sb could be detected only in the working environment. Sn, Ag and Sb are components of the alloys in the melt of the wave solders. In addition to these elements relatively large amounts of Pb and Cu were in the melts. In the melt of the unleaded wave solder the mass concentrations of Sn, Ag, Cu, and Sb (based on the certificate provided by the manufacturer in 2008) were 96.6%, 2.9%, 0.4% and 0.01% respectively. Mass per cent values in the melt of the leaded wave solder for Sn, Pb, Sb, Ag and Cu were 62.8%, 37.0%, 0.02%, 0.1%, and <0.001% respectively.

It can clearly be seen that the lowest concentrations of the alloy elements were detected at the SAV. One of the most abundant elements at the wave solders was Sn which indicated that the emitter was the melt. Cu alloy in the unleaded melt was relatively high, which explains the higher concentration values at the ULWS. The Ag/Sn concentration ratio was 0.05 at ULWS (in 2008) which agreed well with the Ag/Sn ratio in the unleaded melt (in 2008). Since the certificate of the melt was not available in 2009 we could not

Table 1
Concentrations of PM and of elements obtained for coarse samples collected outdoors and in the industrial hall in 2008 and 2009.

	$PM_{2.5-10}$													
	06.10.2008–08.10.2008				27.05.2009–29.05.2009									
	Outdoor (ATOMKI)		Unleaded wave solder		Unleaded wave solder		Leaded wave solder		Store of hazardous materials		Supply air ventilator		Outdoor (ATOMKI)	
	13.7 $\mu g/m^3$ [a]		9.9 $\mu g/m^3$ [a]		5.6 $\mu g/m^3$ [a]		4.3 $\mu g/m^3$ [a]		4.9 $\mu g/m^3$ [a]		5.2 $\mu g/m^3$ [a]		9.3 $\mu g/m^3$ [a]	
	conc.(ng/m^3)	Error	conc.(ng/m^3)	Error (ng/m^3)	conc.(ng/m^3)	Error (ng/m^3)	conc.(ng/m^3)	Error (ng/m^3)	conc.(ng/m^3)	Error (ng/m^3)	conc.(ng/m^3)	Error (ng/m^3)	conc.(ng/m^3)	Error (ng/m^3)
Al	596.3	7.6	117.5	2.6	133.2	5.0	122.4	4.9	110.4	4.4	99.4	4.1	277.1	5.7
Si	1151.0	4.8	136.3	1.8	173.3	1.9	138.9	1.9	89.8	1.8	80.5	1.8	685.4	3.5
P	19.7	2.0	5.1	0.8	8.4	1.1	10.2	1.1	11.3	1.0	6.6	1.0	8.0	1.5
S	152.0	2.0	110.8	1.0	36.9	1.0	35.9	1.0	21.9	0.9	17.9	0.9	74.3	1.5
Cl	42.3	1.6	37.4	0.8	83.0	0.8	78.5	0.8	31.8	0.8	34.8	0.8	63.1	1.3
K	201.8	2.1	79.4	2.0	45.2	1.2	42.8	1.1	18.2	1.0	17.0	0.7	107.8	1.5
Ca	700.1	3.2	95.3	2.3	102.4	1.4	78.7	1.3	33.4	1.1	29.2	0.8	245.4	1.8
Ti	28.7	1.0	5.8	0.4	7.7	0.4	5.7	0.4	2.5	0.3	3.1	0.3	18.1	0.6
Mn	11.1	1.0	1.8	0.3	1.7	0.3	1.1	0.3	0.9	0.2	1.4	0.2	5.1	0.6
Fe	655.4	5.1	180.7	1.4	187.5	1.7	173.8	1.6	137.5	1.4	188.3	1.6	222.2	2.5
Cu	34.6	1.9	8.8	0.5	10.0	0.6	3.2	0.3	2.9	0.3	2.5	0.3	8.5	0.9
Zn	16.9	1.6	14.4	0.7	11.6	0.7	10.2	0.7	5.3	0.5	4.3	0.4	3.3	0.7
Br	<DL	–	6.0	1.5	12.9	1.5	3.5	0.9	2.2	0.7	1.2	0.6	<DL	–
Ag	<DL	–	22.3	1.5	17.1	1.9	20.3	1.9	14.9	1.6	16.9	1.5	<DL	–
Sn	<DL	–	412.4	4.5	98.2	4.9	88.4	4.6	85.5	2.8	23.7	2.5	<DL	–
Sb	<DL	–	<DL	–	<DL	–	<DL	–	<DL	–	<DL	–	<DL	–
Pb	6.8	2.9	34.4	2.0	3.5	1.0	22.9	1.8	45.7	2.3	4.0	0.9	1.5	0.9

[a] PM conc.

Table 2
Concentrations of PM and of elements obtained for fine samples collected at the outdoor site and in the industrial hall in 2008 and 2009.

	$PM_{2.5}$															
	06.10.2008–08.10.2008				27.05.2009–29.05.2009											
	Outdoor (ATOMKI)		Unleaded wave solder		Unleaded wave solder		Leaded wave solder		Store of hazardous materials		Supply air ventilator		Outdoor (ATOMKI)	
	11.4 μg/m³ [a]		8.3 μg/m³ [a]		4.2 μg/m³ [a]		4.6 μg/m³ [a]		5.1 μg/m³ [a]		5.1 μg/m³ [a]		7.5 μg/m³ [a]	
	conc.(ng/m³)	Error (ng/m³)	conc.(ng/m³)	Error (ng/m³)	conc.(ng/m³)	Error (ng/m³)	conc.(ng/m³)	Error (ng/m³)	conc.(ng/m³)	Error (ng/m³)	conc.(ng/m³)	Error (ng/m³)	conc.(ng/m³)	Error (ng/m³)
Al	335.8	5.8	73.8	2.3	64.9	3.1	68.7	3.3	60.7	3.2	58.5	3.1	193.7	4.63
Si	203.2	2.5	40.1	1.6	45.8	1.6	43.8	1.6	38.4	1.6	31.6	1.6	269.7	3.01
P			0.0		2.6	1.1	2.9	1.2	3.9	1.2	4.4	1.1	–	
S	537.7	1.7	274.2	1.0	263.4	1.0	282.0	1.0	267.7	1.0	287.0	1.0	465.7	1.76
Cl	27.7	1.2	12.6	0.8	4.4	0.9	5.6	0.9	2.1	0.9	1.4	0.9	2.5	1.29
K	260.5	1.7	127.9	1.0	17.8	0.6	18.8	0.7	18.0	0.7	18.1	0.6	59.0	1.29
Ca	109.8	1.9	21.5	1.1	13.7	0.6	14.5	0.6	11.9	0.6	8.8	0.5	72.2	1.05
Ti	6.1	0.6	1.1	0.3	<DL	–	0.7	0.3	0.8	0.3	0.7	0.3	8.5	0.52
Mn	7.9	0.7	2.6	0.3	1.2	0.2	1.2	0.2	0.8	0.2	1.1	0.2	2.1	0.52
Fe	353.8	3.5	94.7	1.1	110.4	1.3	124.5	1.3	106.0	1.2	97.3	1.2	111.6	1.74
Cu	15.5	1.2	17.7	0.7	3.1	0.3	2.9	0.3	3.3	0.3	2.4	0.3	8.0	0.77
Zn	38.4	2.1	15.7	0.7	11.3	0.7	9.9	0.7	8.1	0.6	6.2	0.5	5.3	0.77
Br	<DL	–	13.2	1.4	8.2	1.2	6.8	1.1	3.3	0.8	3.9	0.9	<DL	–
Ag	<DL	–	14.8	1.2	10.1	1.3	8.8	1.4	8.0	1.4	8.2	1.3	<DL	–
Sn	<DL	–	85.9	5.5	20.3	2.1	23.3	2.3	22.0	2.2	13.2	2.1	<DL	–
Sb	<DL	–	<DL	–	5.86	2.34	6.34	2.53	5.97	2.37	5.50	1.97	<DL	–
Pb	30.2	3.5	34.3	1.9	2.4	0.8	4.3	1.0	4.1	0.9	2.6	0.8	2.4	1.49

[a] PM conc.

compare the Ag/Sn ratios in 2009. Relatively high Pb concentration at the LWS can be explained by the Pb alloy in the melt of the LWS.

After tin, the concentration of iron was the highest in the workplace. The ratio of Fe/Si (both in the coarse and fine fraction) was higher at the SAV implying a possible Fe source from the SAV or around the SAV. The source of Fe could not be identified from the bulk elemental composition data.

At the wave solders not only were the concentrations of the alloy elements enriched, but increased concentrations of coarse mode Zn, S, K, Cl, P, Br and the crust-related elements were also observed. On the one hand this effect can be understood as the contribution of resuspended dust due to increased working activity around the soldering equipment. On the other hand Zn, Cl, P, K, S and Br may originate from emission sources around the solders.

Among the observed elements, Zn and Cl had the highest indoor/outdoor concentration ratios in this workplace. In addition the highest indoor/outdoor values of them were measured at the wave solders (LWS: $C_{Zn}^{PM_{2.5-10}} = 3.09$, $C_{Zn}^{PM_{2.5}} = 1.86$, $C_{Cl}^{PM_{2.5-10}} = 1.24$, $C_{Cl}^{PM_{2.5}} = 2.24$, ULWS: $C_{Zn}^{PM_{2.5-10}} = 3.51$, $C_{Zn}^{PM_{2.5}} = 2.13$, $C_{Cl}^{PM_{2.5-10}} = 1.32$, $C_{Cl}^{PM_{2.5}} = 1.76$). The most likely explanation is the emission of a flux material, which usually contained $ZnCl_2$ [40]. Most wave solder machines contain a fluxing zone. When a PCB enters this zone the active ingredients of the flux remove surface oxide from the metal components. In commercial wave soldering, a liquid flux is applied to a PCB using a spray dispenser. This process could generate aerosols. A flux activator is typically composed of acid, halide compounds, or combination of both. (e.g. hydrochloric acid, hydrobromic acid, or phosphoric acid) [41]. The increased P concentration at the solders and the Br concentration at the ULW might be explained by the P and Br compounds of the flux activator. The chemical reaction between the $ZnCl_2$ based fluxes and the copper oxide is complex, but it can be described by the following simplified formula [42]:

$$ZnCl_2 + H_2O \rightarrow Zn(OH)Cl + HCl$$

$$CuO + 2HCl \rightarrow CuCl_2 + H_2O$$

Beside the small amount of activator, a conventional soldering flux contains a carrier and other ingredients which protect the clean metal surface from reoxidation. These materials are usually a mixture of chemicals (e.g. alcohols, oils, esters, glycol and water) which contain elements which are not detectable by our macro-PIXE method. Although we did not detect their presence by PIXE, they may have made a significant contribution to the measured mass concentration.

It is interesting that the concentration of the alloy elements of the leaded melts such as Sn and Pb increased at the SHM. Moreover, the coarse Pb concentration at the SHM was two times higher than at the LWS, which suggested that another leaded solder was near to the SHM, and our sampler was accidently placed in the way of the airflow from this wave solder. The second LWS as the source of the excess Pb and Sn was also confirmed by the fact that the concentration ratio of the Pb/Sn was 0.53 which agreed with the Sn–Pb alloy concentration ratio of the Sn–Pb melt at the LWS. The fact that Zn and Cl concentrations were not as high at the SHM as at the solders could be explained by application of a flux with organic activators. It seems that the coarse concentration of P was as high as at the LWS implying similar P additives in the second wave solder.

The higher Pb level at the ULWS in 2008 than at the LWS in 2009 can be explained by the change in technology and the different working hours. From 2008 to 2009 almost all leaded wave solders were changed to unleaded ones, and the air ventilation system became better too. In addition the solders were in operation 24 h per day in 2008, and only 16 h in 2009.

In summary, the values of the both PM fractions (PM_{10} and $PM_{2.5}$) were below the AQ standard values applying to the ambient outdoor air ($PM_{2.5}$: 25 μg/m^3, PM_{10}: 50 μg/m^3) both in 2008 and in 2009. Furthermore, lead concentration values exceeded neither the guidelines of the Occupational Safety and Health Administration (OSHA) nor the WHO. For the lead level, the OSHA standard is 50 μg/m^3 (8-h time-weighted average) [43] while the WHO [44] guideline is 0.5 μg/m^3 annual average.

3.2. Mass size distribution of indoor aerosols

The mass size distribution of some elements measured in October 2008 is illustrated in Fig. 1. Similar results (not detailed here) were found in April 2009. As we mentioned earlier, the sampling took place at the ULWS. Five groups were identified according to the similarities in the size distribution. Al, Si, Ca and Ti composed the first group (Fig. 1a). In the size distribution of these elements two dominant peaks were found: one at the 1–2 μm aerodynamic diameter size range and a second at the 8–16 μm size range. In the outdoor air these elements are of natural (crustal) origin [45].

The second group (Fig. 1b) contained K and S. These elements appeared with high frequency in the 0.25–0.5 μm size range implying that these particles (containing S and K) are generated mainly from combustion processes or photochemical reactions [46]. This size distribution was identical to the size distribution of anthropogenic S and K in the outdoor air, wherein the high amount of K originated from biomass burning in 2008 and S was most probably derived from sulphates.

Only Sn was classified to the third group (Fig. 1c). The concentration of Sn showed an increase towards the coarse mode with the dominant peak at the 8–16 μm size range. It was clearly seen that Sn particles were emitted from the solders in a wide size range and the most abundant mass appeared at the 8–16 μm range.

Elements of the fifth group (Fig. 1d and e) were related to the soldering and the fluxing process: Cu, Cl, Ag, Pb, Zn, Mn and Br. Among these elements Cl, Ag, Cu and Pb showed a bimodial shape (Fig. 1d) with one wide peak in the 0.25–1 μm range and another in the 8–16 μm range. The Ag, Cu, Pb, Cl, and Zn concentrations corresponding to the 0.25–1 μm region originated from the evaporation of the hot melt and the metal oxides dissolved in the flux ($ZnCl_2$). Part of the wide fine peak is within the droplet mode [47] (0.5–1.0 μm). As we mentioned earlier spray fluxing is a commonly used technique for PCB manufacturing, which produces liquid droplets in the aerosol size range. The occurrence of the Ag, Cu, Pb in droplet mode can be explained by the reaction of metal vapours (from the melt) with the droplets of the flux. The reaction between Ag, Cu, Pb metals and the flux was also confirmed by the positive correlations between the Zn concentration and the concentrations of Cl, Pb, and Cu (Fig. 2a–c). Ag and Cl concentrations also exhibit good correlation in the fine size range (Fig. 2f). Both Mn and Br had a dominant peak in the fine fraction (Fig. 1e). On the other hand a smaller maximum was at the coarse fraction in the Br size distribution. This latter peak agreed with the peak of the Zn. Based on the correlation between Zn, Mn and Br (Fig. 2d and e) these elements were related to the fluxing procedure, too. The fact that Ag and Pb were alloy elements in the melts explained the peak in the coarse mode (8–16 μm size range). This was confirmed by the correlation between Sn concentration and Ag and Pb concentrations (Fig. 2g and h) and by the ratio of Ag/Sn (at 8–16 μm) which agreed with the Ag/Sn ratio of the unleaded melt.

In the last group iron appeared in a wide interval (0.25–8 μm) and showed high concentration at the 1–2 μm size. Two smaller peaks can also be seen on the mass size distribution: one was at 0.5–1 μm and the other at the 8–16 μm size range. These were the size ranges where the crust-related elements had peaks (Fig. 1f). Since Fe is also a crust-related element, one part of the measured

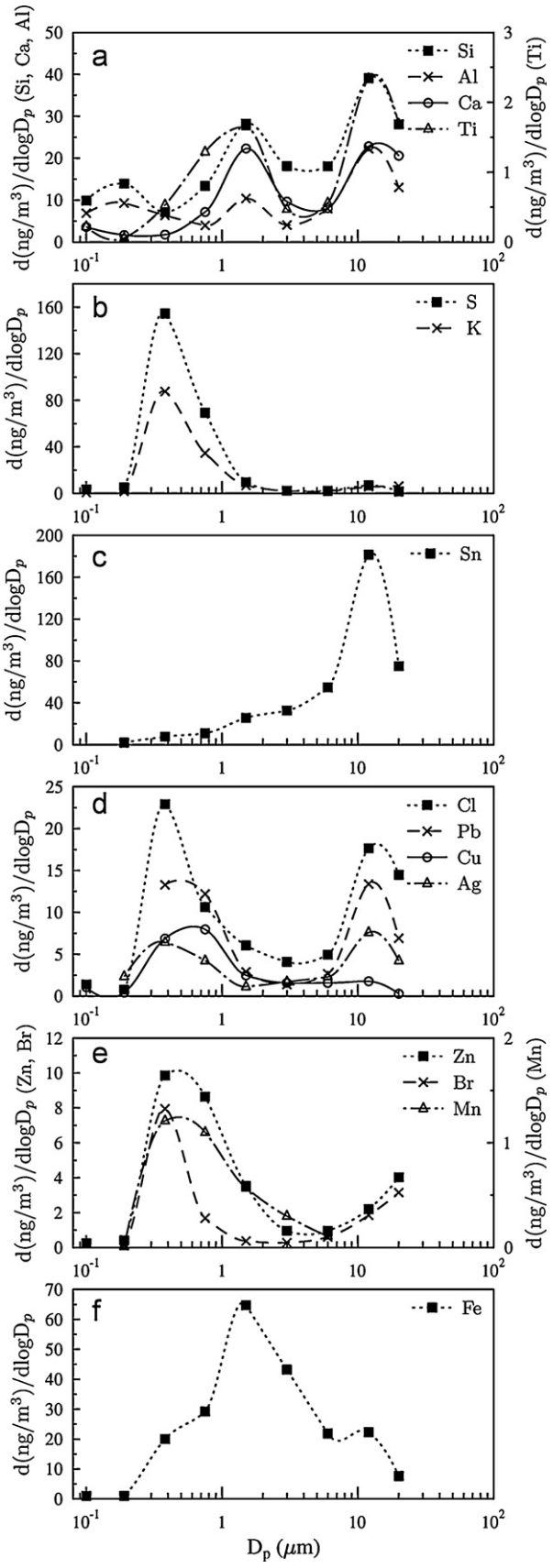

Fig. 1. Mass size distribution of certain elements (sampled in the workplace in 2008) separating for five groups: (a) Group 1; (b) Group 2; (c) Group 3; (d) Group 4; (e and f) Group 5.

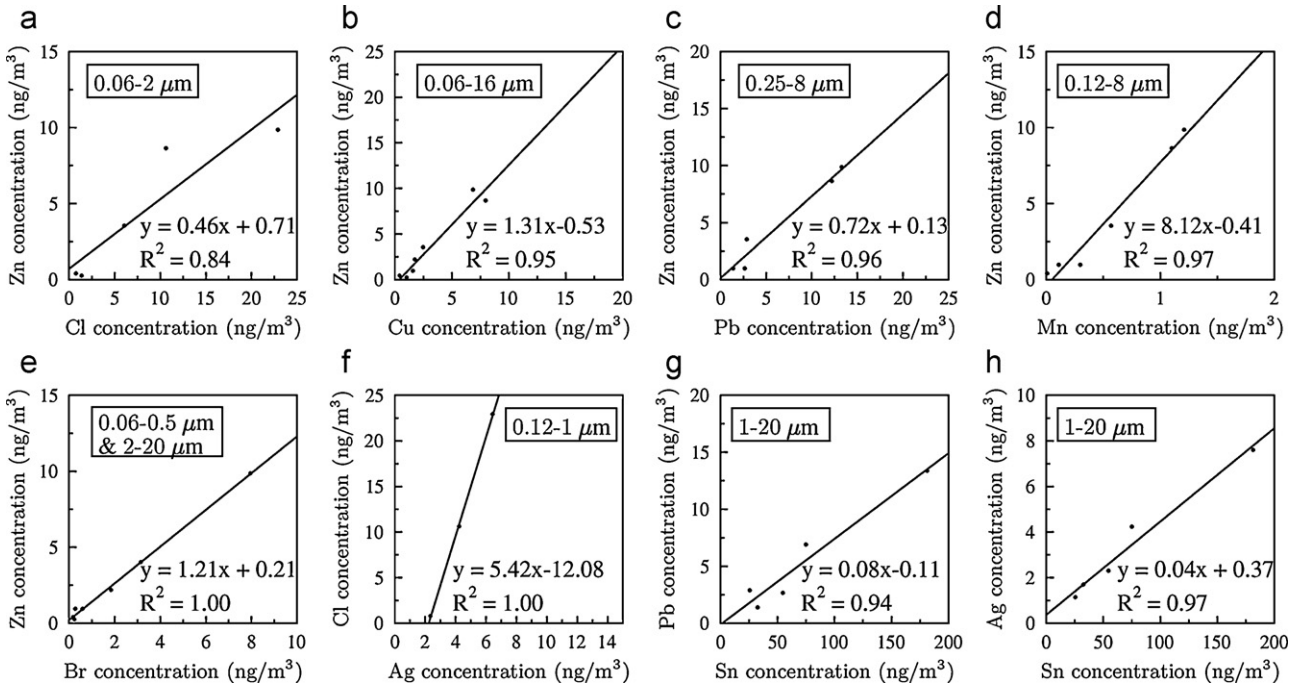

Fig. 2. Relationships between the elemental concentrations measured in the different size fractions. Each point represents a single size range of the mass size distribution. The numbers in the left corner indicate the wider size ranges in which the correlation stands.

Fe was attributed to the outer air. However, the curve shape indicates that Fe had at least one other indoor source which made a significant contribution in the fine fraction.

3.3. Single particle analysis with proton microprobe and scanning electron microscopy

Additional information concerning the characteristics of the aerosol particles was drawn from individual particle analysis by scanning nuclear microscopy and SEM. In order to determine the composition of the particles, ion microprobe analysis was carried out. The quantitative elemental composition of ~200 particles with different sizes was determined. The size of the particles covered the 0.25–20 μm range.

A great number of the investigated particles were iron-rich. The single particle analysis showed that there was a strong correlation between Fe and Cl ($r = 0.87$, $p < 0.001$) in the particles with great size variability (0.25–2 μm and 8–16 μm). Based on the morphology images, we found that the particles within the 8–16 μm range consisted of agglomerated Fe–Cl particles (Fig. 3a). In this size range, some Fe–Cl particles contained Na too. One reasonable explanation for the Fe–Cl particles might be the so-called etching process with a $FeCl_2$ solution [48], which is a preceding process in PCB manufacturing. During this milling procedure the unwanted brass foil which covers the PCBs is etched away in the iron(III) chloride solution [49]:

$$FeCl_3 + Cu \rightarrow FeCl_2 + CuCl$$

$$FeCl_3 + CuCl \rightarrow FeCl_2 + CuCl_2$$

In addition, it is commonly used in the etching process in a way that the etchant is sprayed perpendicular to the copper surface, which facilitates the generation of aerosols.

However, $FeCl_2$ accounts for only part of the Fe-rich particles in the 1–2 μm size range, in which Cl concentrations did not show maximum values. Iron rich particles of 1–4 μm diameter also contained a high amount of Sn accompanied by Al, Si, Ca and minor amounts of Mn, Zn, Pb and Cu. Another main component (30–40% by weight) of these particles was O. Many particles which contained only Fe and O (see Fig. 3b) were found in the SEM analysis. Since we were not able to visit all areas of the workplace (due to manufacturing secrecy) the origin of the indoor Fe–O particles remained unclear. The high Fe–O emission in the workplace, the outer Fe–O and some particles consisting of $FeCl_2$ together resulted in the dominant peak at the 1–2 μm range in the size distribution of Fe (see Fig. 1f).

Beside the Fe–Cl correlation, we found that Zn and other metals such as Pb, Sn, Br, Mn, Cu showed strong correlation ($r = 0.911$, 0.643, 0.915, 0.764, 0.842 respectively; all p values were lower than 0.01) with Cl in the particles with a size of less than 1 μm. The Zn–Cl correlation attributed to the flux materials which contained $ZnCl_2$ and the metal-Cl correlations could be explained by the powerful reactivity of the chlorine originating from fluxing. Strong correlation was also observed between Cl and Na in the particles larger than 2 μm. The highest concentration of Na and Cl were in the particles with a size larger than 8 μm. The source of these particles might have been a detergent which contained sodium and chloride. In Hungary, there is a commonly used detergent containing NaOCl (<5%), NaCl and NaOH (0.5–2%). Probably the salt and NaOH were also responsible for the Na content of the large Fe–Cl particles (see Fig. 3c). The detergent and the $FeCl_2$ emission from milling were responsible for the coarse fraction peak in the Cl size distribution.

The micro-PIXE analysis also showed that Cl, Cu and Pb correlated (Cu–Pb: $r = 0.614$, $p < 0.01$) with each other in the 0.25–1 μm size range. One of these particles is shown in Fig. 3d, which presents spheroidal morphology on the left side and well-defined edges on the other side of the particle. Since Pb and Cu were alloy elements in the melt of the solders, Pb, Cu and Cl probably became associated via interaction of the melt particles with the flux fluid.

Another large group of particles were those which contained Sn in large concentration. Some of these were associated with Fe-rich particles in the fine fraction, as we mentioned earlier. On the other hand, Sn particles of spheroidal morphology with smooth

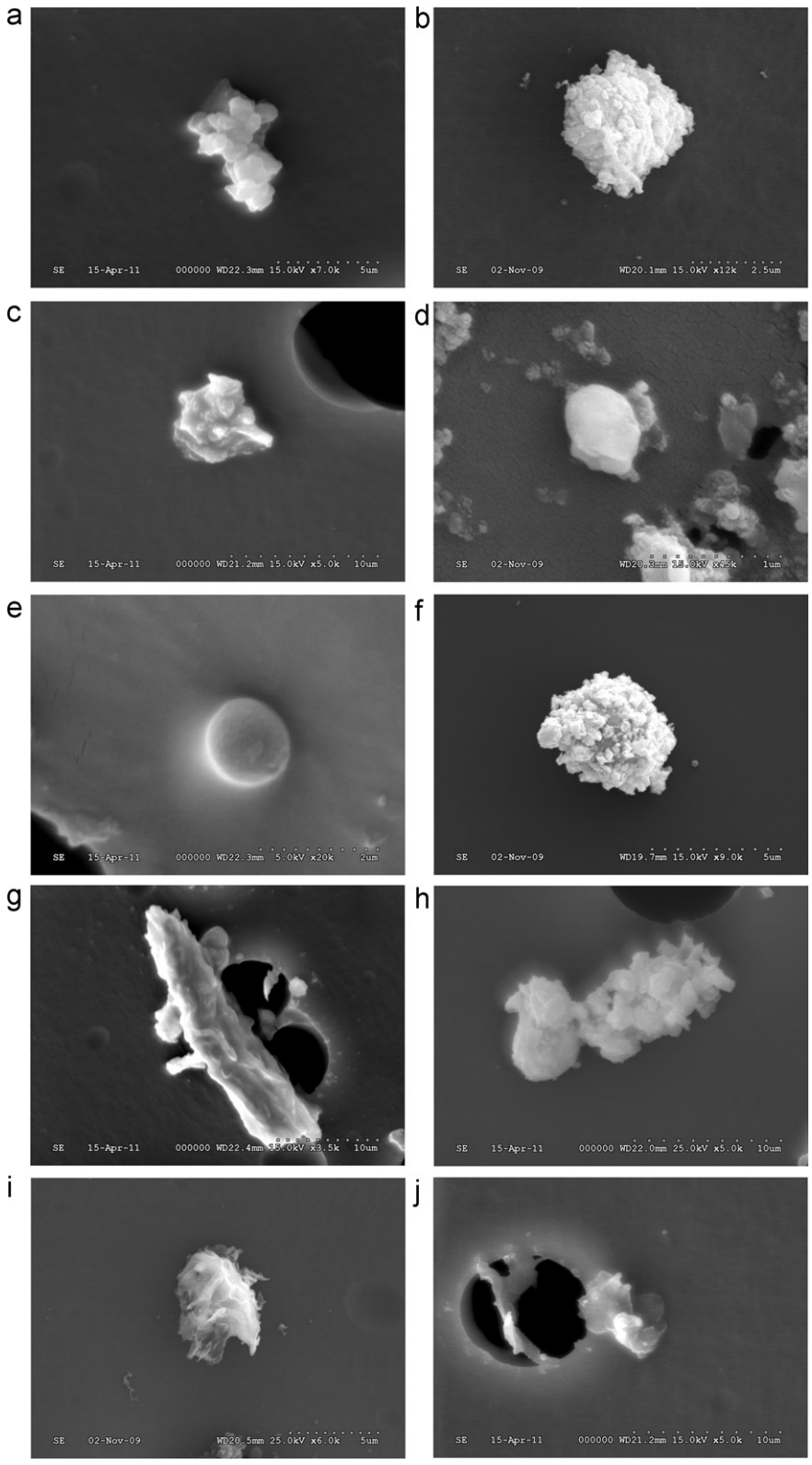

Fig. 3. SEM image of typical aerosol particles. (a) Agglomeration of Fe–Cl rich particles; (b) iron oxide; (c) Fe–Cl rich particle with Na; (d) Pb–Cu–Cl particle; (e) Sn particle with spheroid morphology; (f) Sn particle with sub-particles on surface; (g) Sn–Ag particle of ULWS origin; (h) Sn–Pb aggregates derived from the LWS; (i) Sn particle with irregular morphology; (j) Zn rich particle.

texture were also observed (Fig. 3e). The presence of these particles was due to evaporation processes. They were generated in high-temperature processes, obviously from a wave solder of the working hall. In the coarse fraction Sn particles with spheroid morphology were also found (Fig. 3f). It can be seen that it has a well-defined spheroid core with small particles attached to the surface. Moreover, some of the Sn-rich particles were crystallized in an elongated shape (Fig. 3g) or they were aggregates (Fig. 3h), while some had an irregular form (Fig. 3i). These particles consisted of the alloy elements.

Table 3
Depositions in the extrathoracic (eth.), tracheobronchial (bron.) and the acinar (acin.) part of the respiratory system in % for Pb, Sn, Fe and S elements (sampled at the ULWS in 2008).

	Male				Female			
	Extrathoracic (%)	Bonchial (%)	Acinar (%)	Sum. (%)	Extrathoracic (%)	Bonchial (%)	Acinar (%)	Sum. (%)
Under sitting								
Pb	47.7	2.20	10.60	60.50	45.6	2.21	7.33	55.14
Sn	80.4	2.2	5.34	87.94	77.7	2.77	4.40	84.87
Fe	40.7	3.36	14.3	58.36	35.6	3.48	10.2	49.28
S	14.6	2.11	10.90	27.61	14.50	1.91	7.10	23.51
Under light exercise								
Pb	57.1	1.96	7.72	66.78	55.2	1.95	7.34	64.49
Sn	87.1	1.05	3.07	91.22	86.2	1.18	3.1	90.48
Fe	54.5	2.6	9.67	66.77	51.6	2.70	9.32	63.62
S	17.8	1.91	10.2	29.91	16.80	1.88	9.31	27.99

Both the micro-PIXE and the SEM analysis observed Zn-rich particles in the coarse fraction (Fig. 3j) which were associated with crust-related particles and some of them with Cl and Br. This result confirmed the observed Zn peak at the coarse fraction.

3.4. Stochastic lung model calculations

Based on the size distribution data, the deposition probabilities of the different particle types were calculated within the human respiratory system with the above mentioned stochastic lung deposition model. The model separates the respiratory system into three main regions: the extrathoracic, traceobronchial and acinar regions.

Results of the calculations for 4 highlighted elements according to the different size distributions are shown in Table 3. It can be seen that the higher the per minute ventilation the higher the ratio of total deposition i.e. the deposition was higher for males (by about 1–15%) than for females and higher during light exercise (by 8–15%) than during sitting. Furthermore, in all cases the highest deposition fraction was in the extrathoracic region. The fact that the total deposition fraction was higher for light exercise than for sitting can be explained by the faster breathing frequency and shallower inhalation. The total deposition rate was highest (between 85% and 91%) in the case of Sn, which was found with high concentration in the coarse mode, and the extrathoracic deposition played a significant role. The explanation for this is that the filtration process of the extrathoracic region is rather effective i.e. the majority of these coarse particles are trapped before or in the bronchial region. Despite the different size distribution of Pb and Fe, the total deposition of these elements were similar. However, the deposition of Pb was higher than the Fe deposition in the extrathoracic region, while the deposition rate of Fe was higher in the acinar region. Furthermore, it was found that the total deposition of Pb (which is very important from the point of toxicity) was about 55–67%, which meant that more than half of these particles entered the human respiratory system and stayed there for a shorter or longer time. The calculated doses of Pb were 179.55 μg (in 2008) and 15.42 μg (in 2009) for an adult male under sitting during one shift (8 h). Nevertheless, the majority of these particles remained in the extrathoracic region, whose cleaning mechanism is fast and effective. The total deposition was lowest (between 24% and 30%) in the case of S, but almost a third of these particles reached the acinar region from where they can easily get into the bloodstream.

4. Summary

In this study a complex survey of the aerosol pollution of the production hall of an electronic products company was presented. It was confirmed that relative to the outdoor atmosphere inside the working hall the air was clean. The PM concentration values and the lead concentration were far below the WHO guidelines. Despite the continuously working air-filtering equipment we were able to identify aerosol particles of outdoor origin in the working area: e.g. aluminium-silicate minerals, KCl from biomass burning or fertilizing, K_2SO_4, Ca–P from fertilizing or industry. However, the aerosols created indoors contributed the major part of the PM concentration measured in the hall. Based on the elemental ratios and correlations, size distribution data and single particle analysis, the creation processes and the indoor sources were identified, e.g. soldering, fluxing, etching and cleaning. The concentration of PM and the elemental components increased at the wave solders. The main constituents of the leaded and the unleaded melt were recognized in the indoor aerosols. In the case of PM_{10}, the Pb levels in the workplace were approximately 3.8 times higher on average than the outer Pb levels. Flux-related and etching-related elemental compositions were also identified. Although the concentrations of Pb were less than the limit value of the OSHA and WHO, there was a maximum in the fine mode in the mass size distributions of Pb and other metals which increase the risk of adverse effects. Based on the stochastic lung model calculations, the majority of the observed elements are deposited in the extrathoracic regions. The total deposition fraction was higher for light exercise than for sitting, but the deposition in the (deeper) acinar region was higher in the case of sitting.

The differences between the two sampling periods could be attributed to the change in technology and working schedule. From 2008 to 2009 most of the leaded wave solders were put out of operation, which could be detected through the decrease in lead concentration. However, parallel to this other melt components and fluxing materials containing transitional metals, heavy metals and organic compounds were introduced, which lead to the presence of Cl, Zn, Ag and Br, among others. Their effect on health has not yet been studied.

Acknowledgements

This work was supported by the Hungarian Research Fund OTKA and the EGT Norwegian Financial Mechanism Programme (contract no. NNF78829) and the János Bolyai Research Scholarship of the Hungarian Academy of Sciences.

References

[1] A.P. Jones, Indoor air quality and health, Atmos. Environ. 33 (1999) 4535–4564.
[2] J.Q. Koenig, T.F. Mar, R.W. Allen, K. Jansen, T. Lumley, J.H. Sullivan, et al., Pulmonary effects of indoor- and outdoor-generated particles in children with asthma, Environ. Health Perspect. 113 (2005) 499–503.
[3] E. Horak, B. Morass, H. Ulmer, Association between environmental tobacco smoke exposure and wheezing disorders in Austrian preschool children, Swiss Med. Wkly. 137 (2007) 608–613.

[4] T.M.C.M. deKok, H.A.L. Driece, J.G.F. Hogervorst, J.J. Briede, Toxicological assessment of ambient and traffic-related particulate matter: review of recent studies, Mutat. Res./Rev. Mutat. Res. 613 (2006) 103–122.
[5] F. Laden, L.M. Neas, D.W. Dockery, J. Schwarts, Association of fine particulate matter from different sources with daily mortality in six U.S. cities, Environ. Health Perspect. 108 (2000) 941–947.
[6] H. Ormstad, Suspended particulate matter in indoor air: adjuvants and allergen carriers, Toxicology 152 (2000) 53–68.
[7] R.E. Lee, D.J. Lehmden, Trace metal pollution in environment, J. Air Pollut. Control Assoc. 23 (1973) 853–857.
[8] D. Wake, D. Mark, C. Northage, Ultrafine aerosols in the workplace, Ann. Occup. Hyg. 46 (S1) (2002) 235–238.
[9] R.L. Davidson, D.F.S. Natusch, J.R. Wallace, C.A. Evans, Trace elements in flash, Environ. Sci. Technol. 8 (1974) 1107–1113.
[10] G. Buonanno, L. Morawska, L. Stabile, Exposure to welding particles in automotive plants, J. Aerosol Sci. 42 (2011) 295–304.
[11] J. LaDou, Printed circuit board industry, Int. J. Hyg. Environ. Health 209 (2006) 211–219.
[12] P.V. Offermann, C.J. Finley, Metal fume fever, Ann. Emerg. Med. 21 (1992) 872–875.
[13] R. Quansah, J.J.K. Jaakkola, Paternal and maternal exposure to welding fumes and metal dusts or fumes and adverse pregnancy outcomes, Int. Arch. Occup. Environ. Health 82 (2009) 529–537.
[14] M.I. Schwarz, T.E. King, Interestial Lung Disease, People's Medical Publishing House, USA, 2009.
[15] P. Howe, P. Watts, Tin and Inorganic Tin Compunds, WHO, 2005.
[16] L.W. Chang, Toxicology of Metals, CRC Lewis Publishers, Boca Raton, FL, 1996.
[17] M.S. Golub, Metals Fertility, and Reproductive Toxicity, CRC Press is an imprint of Taylor & Francis Group, 2006.
[18] M.M. Aral, Environmental Modeling and Health Risk Analysis (Acts/Risk), Springer, New York, 2010, pp. 97–98.
[19] R. Lilis, A. Fischbein, J. Eisinger, Prevalence of lead disease among secondary lead smelter workers and biological indicators of lead exposure, Environ. Res. 14 (1977) 255–285.
[20] K. Mitzner, Complete PCB Design Using Or CAD Capture and Layout, Elsevier Inc., Burlington, 2007.
[21] K.J. Puttlitz, K.A. Stalter, Handbook of Lead-Free Solder Technology for Microelectronic Assemblies, Marcel Dekker Inc., New York, 2005, pp. 37–45.
[22] L. Koblinger, W. Hofmann, Monte Carlo modeling of aerosol deposition in human lungs. Part I: simulation of particle transport in a stochastic lung structure, J. Aerosol Sci. 21 (1990) 661–674.
[23] C.J. Hegedűs, I. Balásházy, Á. Farkas, Detailed mathematical description of the geomerty of airway bifurcations, Respir. Physiol. Neurobiol. 141 (2004) 99–114.
[24] I. Balásházy, I. Németh, B. Alföldy, P.P. Szabó, C. Hegedűs, W. Hofmann, J. Pálfalvy, I. Fehér, S. Török, Aerosol deposition modelling in human airways and alveoli, J. Aerosol Sci. 31 (2000) 482–483.
[25] www.pixeintl.com/Impactor.asp.
[26] P.K. Hopke, Y. Xie, T. Raunemaa, S. Biegalski, S. Landsberger, W. Maenhaut, P. Artaxo, D. Cohen, Characterization of the gent stacked filter unit PM10 sampler, Aerosol Sci. Technol. 27 (1997) 726–735.
[27] W. Maenhaut, K.G. Malmquist, Particle.induced X-ray emission analysis, in: R.E. van Grieken (Ed.), Handbook of X-ray Spectrometry, 2nd ed., Marcel Dekker, Inc., 2001.
[28] I. Borbély-Kiss, E. Koltay, S. László, G. Szabó, L. Zolnai, Experimental and theoretical calibration of a PIXE setup for K and L X-rays, Nucl. Instrum. Methods Phys. Res. B: Beam Interact. Mater. Atoms 12 (1985) 496–504.
[29] I. Rajta, I. Borbély-Kiss, G. Mórik, L. Bartha, E. Koltay, Á.Z. Kiss, The new ATOMKI scanning proton micropobe, Nucl. Instrum. Methods Phys. Res. B: Beam Interact. Mater. Atoms 109 (1996) 148–153.
[30] I. Uzonyi, G. Szabó, I. Borbély-Kiss, Á.Z. Kiss, Calibration of an UTW Si(Li) detector in the 0. 28–22.1 keV energy range at a nuclear microprobe, Nucl. Instrum. Methods Phys. Res. B: Beam Interact. Mater. Atoms 210 (2003) 147–152.
[31] I. Uzonyi, I. Rajta, L. Bartha, Á.Z. Kiss, A. Nagy, Realization of the simultaneous micro-PIXE analysis of heavy and light elements at a nuclear microprobe, Nucl. Instrum. Methods Phys. Res. B: Beam Interact. Mater. Atoms 181 (2001) 193–198.
[32] Z. Kertész, Z. Szikszai, I. Uzonyi, A. Simon, Á.Z. Kiss, Development of a bio-PIXE setup at the Debrecen scanning proton microprobe, Nucl. Instrum. Methods Phys. Res. B: Beam Interact. Mater. Atoms 231 (2005) 106–111.
[33] G. Szabó, I. Borbély-Kiss, PIXYKLM computer package for PIXE analyses, Nucl. Instrum. Methods Phys. Res. B: Beam Interact. Mater. Atoms 75 (1993) 123–126.
[34] G.W. Grime, M. Dawson, Recent developments in data acquisition and processing on the Oxford scanning proton microprobe, Nucl. Instrum. Methods B 104 (1995) 107–113.
[35] I. Uzonyi, G. Szabó, PIXEKLM-TPI–a software package for quantitative elemental imaging with nuclear microprobe, Nucl. Instrum. Methods Phys. Res. B: Beam Interact. Mater. Atoms 231 (2005) 156–161.
[36] I. Balásházy, A. Horváth, Z. Sárkány, Á. Farkas, W. Hofmann, Simulation and minimisation of airway deposition of airborne bacteria, Inhalation Toxicol. 21 (2009) 1021–1029.
[37] I. Balásházy, B. Alföldy, A.J. Molnár, W. Hofmann, I. Szıke, E. Kis. Aerosol drug.
[38] International Commission on Radiological Protection (ICRP), 1994. Human Respiratory.
[39] Hungarian Air Quality Monitoring System (www.kvvm.hu/olm/).
[40] M. Judd, K. Brindley, Soldering in Electronics Assembly, Reed Educational and Professional Publishing Ltd., Oxford, 1999, pp. 94–108.
[41] M.L. Minges, Electronic Material Handbook, ASM International, 1989, pp. 644–645.
[42] G. Humpston, D.M. Jacobson, Principles of Soldering, ASM International, United States of America, 2004, pp. 116–119.
[43] Code of Federal Regulations, OSHA (Occupational Safety and Health Administration) lead standard. 29 CFR, Part 1910.1025, U.S. Government Printing Office Federal Register, Washington, DC, 1992.
[44] W.H.O., Air Quality Guidelines, World Health Organization, Geneva, Switzerland, 2000.
[45] I. Borbély-Kiss, E. Koltay, G. Szabó, L. Bozó, K. Tar, Composition and sources of urban and rural atmospheric aerosol in Eastern Hungary, J. Aerosol Sci. 30 (1999) 369–391.
[46] L. Morawska, J.J. Zhang, Combustion sources of particles. 1. Health relevance and source signatures, Chemosphere 49 (December) (2002) 1045.
[47] P. Kulkarni, Aerosol Measurement: Principles, Techniques, and Applications, Published by Wiley and Sons, Inc., Hoboken, New Jersey, 2011, pp. 1–704.
[48] C.F. Coombs, Printed Circuits Handbook, McGraw-Hill Companies, United States of America, 2008, pp. 34.17–34.20.
[49] R.S. Khandpur, Printed Circuits Boards: Design, Fabrication, Assembly and Testing, Tata McGraw-Hill Publishing Company Limited, New Delhi, 2005, pp. 365–368.